Analysis of Isothermal Annular Jets: Comparison of Computational Fluid Dynamics and Experimental Data

Eric M. Moore, Robert L. Shambaugh, Dimitrios V. Papavassiliou

School of Chemical Engineering and Materials Science, University of Oklahoma, Norman, Oklahoma 73019

Received 27 January 2004; accepted 17 May 2004
DOI 10.1002/app.20963
Published online in Wiley InterScience (www.interscience.wiley.com).

ABSTRACT: A computational fluid dynamics technique was developed for the simulation of airflow through an annular jet. The technique used a commercial simulation package with a Reynolds stress model for the simulation of turbulent flows. The model parameters were calibrated using available experimental data for circular and annular jets. It was found that, after this calibration, the computational results agreed well with experimental data (specifically, with the velocity magnitude, velocity decay rate, and the velocity spreading rate). The jet geometry studied was based on industrial melt-blowing nozzles. The velocities studied varied from the low subsonic incompressible range to nearly sonic conditions. Based on both the computational and experimental results, a correlation was proposed that predicts the centerline velocity profiles in both the near- and far-field regions. © 2004 Wiley Periodicals, Inc. J Appl Polym Sci 94: 909–922, 2004

Key words: computer modeling; fibers; melt; drawing; thermoplastics

INTRODUCTION

Melt blowing is a process for manufacturing polymer fibers. In melt blowing, streams of hot gases (usually air) attenuate a molten polymer stream into a fine fiber. The fibers are generally collected as a mat on an open screen and that fiber mat is referred to as a nonwoven structure. There are different die geometries that are used to create melt-blown fibers. The two most commonly used dies are slot dies (commonly called Exxon dies; see Harding et al.[1]) and annular dies (often called Schwarz dies; see Schwarz[2]). Slot dies are dies where the air is sent through a pair of long linear slots located on opposite sides of a row of polymer outlets. Typically, the air slots are of the order of 1 mm wide, and the two slots are located about 1 mm apart; however, the length of a slot die is about 0.5 to 3 m. Annular dies are dies where a single annular air outlet surrounds each polymer outlet; generally, there are several rows (three to five) of polymer outlets. A diagram of one hole of an annular melt-blowing die is pictured in Figure 1. Annular melt-blowing dies typically have inner (air) diameters of around 1 mm and outer (air) diameters of about 2 mm.

Recently, slot dies have been studied with a combination of computational fluid dynamics (CFD) analysis and comparison to experimental data[3,4]; slot dies have also been studied with a large eddy simulation approach.[5] Krutka et al.[3] found that the default turbulence model parameters [the parameters suggested within the software (Fluent[6])] need to be modified to obtain agreement between the CFD results and experiments. The present study explores the development of a CFD technique for analyzing flow patterns of isothermal air emanating from an annular orifice. The goal was to develop a method for investigating annular melt-blowing dies without going through the considerable expense of constructing and testing physical dies. The technique is calibrated against the annular jet experimental data of Uyttendaele and Shambaugh[7] as well as other experimental data on circular jets.[8]

The efficiency of the melt-blowing process depends on the behavior of both the air flow field and the polymer stream. The analysis performed here is focused on the air flow field and does not include the effects of the polymer on the air flow field. This approximation is consistent with available experimental data and with models already developed for the melt-blowing process.[9,10] This decoupling of the air and polymer flow leads to a significant reduction in computational and modeling effort, while providing a valuable tool for process development. The implicit assumption, when decoupling the air and polymer flow fields, is that the polymer stream has a slight effect on the air flow field. Because of the rapid attenuation and small diameters of the fibers involved, this appears to be a good approximation when the fibers are beyond the immediate vicinity of the die face (where the fiber diameter is quite large) and away

Correspondence to: R. Shambaugh.
Contract grant sponsor: 3M Company.
Contract grant sponsor: Procter & Gamble.
Contract grant sponsor: ConocoPhillips.

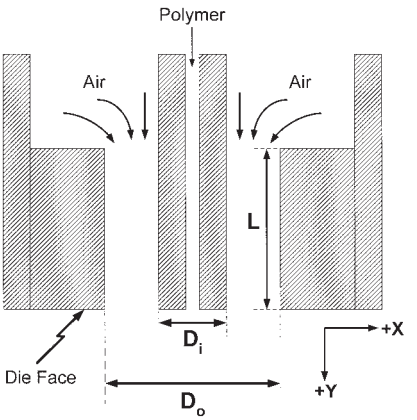

Figure 1 Cross-sectional view of the annular melt-blowing die. The origin of the coordinate system is in the plane of the die face and at the center of the polymer outlet.

from the fiber collection device (given that the collection device can interfere with the air flow pattern).

Circular jets have been studied extensively, although much less work has been done with annular jets. Schlichting[11] presents a theoretical analysis of turbulent circular jets. Ferdman et al.[12] reported that the far-field development of circular turbulent jets is independent of the initial jet velocity profile. This result suggests that annular jets may, at least in the far-field region, behave in a manner similar to that of a turbulent circular jet.

The contributions of the present article are (1) the determination of the turbulence model parameters that need to be used for the successful simulation of an annular air jet, (2) the development of predictive correlations that describe the behavior of the mean air velocity field in annular jets used for melt blowing, and (3) the prediction of turbulence quantities below annular air jets.

EXPERIMENTAL

Computational domain and grid generation

The seven different types of dies simulated in this work included a circular jet and six different annular jets. The first four dies are referred to as Die A, Die B1 (the circular jet), Die B3, and Die B5; this nomenclature is consistent with the work of Majumdar and Shambaugh.[13] Experimental data are available for these four dies.[7,13] The remaining three computational dies are referred to as Die C, Die D, and Die E. For all seven dies, the outer diameters vary from 1.25 mm (Die C) to 3.5 mm (Die E). Inner diameters vary from zero (Die B1) to 2.25 mm (Die D). Table I shows the dimensions of all the dies studied in this work. It is important to note that Die B1 is a circular die used to compare the behavior of a circular jet to an annular jet with the same outer diameter (Die B3). The experimental orifices had different inlet lengths ("L" on Fig. 1) that ranged from 2.70 to 9.36 mm; however, it was experimentally determined that, over the inlet length range used, the length had little effect on the jet development.[7] Other researchers[8,14] found that inlet length does have an effect on jet development in circular jets, but only when inlet lengths are greater than those used in the experimental work of Uyttendaele and Shambaugh[7] (our simulations used lengths of the order of those used by Uyttendaele and Shambaugh).

TABLE I
Die Dimensions and Grid Sizes Used

Die	D_o (mm)	D_i (mm)	Fraction open area[a]	Grid size (cells)
A	2.37	1.30	0.699	58,850
B1	2.46	0.00	1.000	61,150
B3	2.46	1.27	0.733	59,950
B5	1.89	1.27	0.548	59,350
C	1.25	0.45	0.870	58,300
D	2.75	2.25	0.331	58,100
E	3.50	0.50	0.980	60,300

[a] Unitless.

In our present work, the computational grid was created with an inlet length of 5 mm, and the starting velocity profile was assumed to be flat (plug flow). The software used for the CFD calculations was FLUENT® Version 6 from Fluent, Inc.[6] To develop a model for the annular jet flow, a proper computational domain and grid was developed (using Gambit®, which is also from Fluent, Inc.). The coordinate system origin was placed in the plane of the die face and at the center of the annulus. The positive y (axial) axis was aligned with the dominant flow and the x (radial) axis was perpendicular to the y-axis (see Fig. 2). Because the flow geometry involved axisymmetric flow, the FLUENT axisymmetric solver was used. This solver mechanism uses a two-dimensional grid to model the three-dimensional jet using the inherent axial symmetry of the problem. This two-dimensional grid greatly

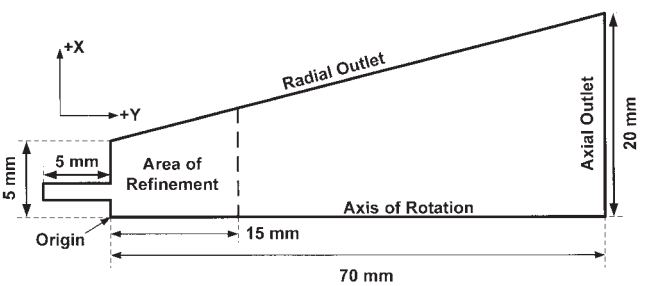

Figure 2 Computational domain used for the simulations. Note that this figure is rotated 90° relative to Figure 1. Thus, the left side of this figure corresponds to the top of the flow field, whereas the right side of the figure corresponds to the bottom of the flow field.

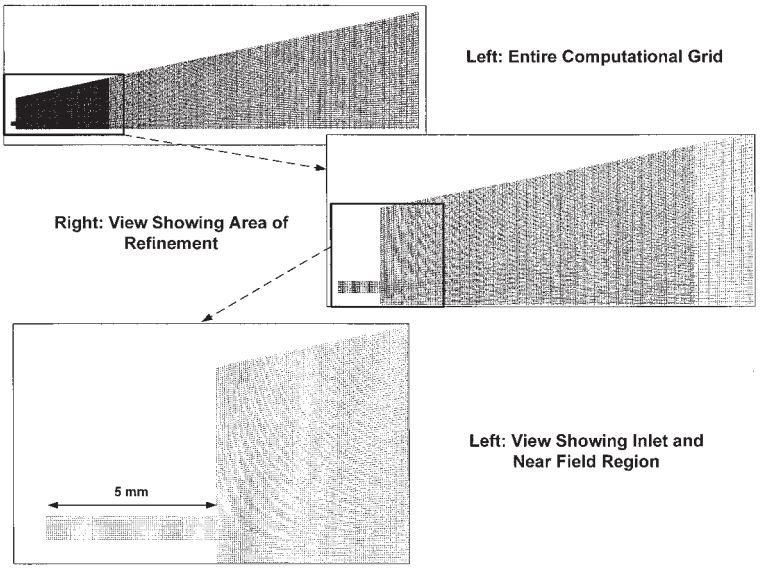

Figure 3 Actual grid used for simulations with Die B3. The width of the jet inlet shown is 0.595 mm (this inlet is the 5 mm long inlet shown in the bottom left of the figure).

reduced the computation time necessary for convergence. The computational domain was defined as a frustum with dimensions sufficient to bound the jet over the region of jet development. In the vertical (y) direction, the domain ran from the jet inlet and on into the fully developed region. Based on the experimental measurements of Uyttendaele and Shambaugh,[7] the overall length of the computational grid was 75 mm (5 mm for the inlet region plus 70 mm for the jet region). In the x-direction (the radial direction as shown in Fig. 2), the experimental measurements of Uyttendaele and Shambaugh were also used to define the active zone of jet development: the upper surface containing the orifice was given a radius of 5 mm, and the radius of the lower surface was set at 20 mm. Uyttendaele and Shambaugh did their experimental measurements of air flow without the presence of a fine polymer stream (see Fig. 1). Likewise, in our simulations we ignored the presence of a polymer stream.

The inlet to the region (at the far left of Fig. 2) was defined as a mass flow inlet; the "height" of this inlet was only $(D_o - D_i)/2$. The two outlets (shown as "radial outlet" and "axial outlet" in Fig. 2) were defined as pressure outlets at atmospheric conditions. The upper (located at the left in Fig. 2) surfaces—both the inlet walls and inlet face—were defined as solid walls. The air was modeled as an ideal gas with constant viscosity. At the relatively low pressures involved in the simulation, the ideal gas model adequately accounts for compressibility. Constant viscosity was assumed because of the nearly isothermal nature of the flow. Because an ideal gas model was used, energy boundary conditions also had to be specified. All walls and outlets were defined at a constant 300 K, and the inlet total temperature was defined such that the static temperature of the inlet air was 300 K. It is important to note that the flow solution is not entirely isothermal. Near the jet inlet there are some thermal variations attributed to both the viscous dissipation and the expansion of the air as it exits the inlet. At higher flow rates these changes become larger as a result of the increased inlet pressure of the air and increased velocity gradients present in the flow.

A grid consisting of rectangular cells was developed to provide accurate answers within reasonable computational time. Grid generation was handled by the Gambit program from Fluent, Inc. For the different dies, the number of cells within each grid was slightly different because of the different die geometries. Table I lists the number of cells used in each grid. Grid generation was conducted by first creating an initial coarse grid; then, the grid was refined in the region closest to the jet orifice. The refinement was done throughout the inlet and on all cells up to 15 mm away from the die face for the entire width of the domain. Figure 3 shows one of the grids used. To test for grid dependency, three additional cases were run on grids that had different levels of refinement. These additional grids had 23,644, 130,009, and 235,400 cells. The centerline velocity results for the grids were compared (see Fig. 4). Because the 58,850 cell grid showed results nearly identical to those of the larger two grids—and substantial differences from the 23,644 cell grid—the 58,850 cell grid was deemed large enough to be grid-independent, and our subsequent work used this grid size.

Simulations with four different air inlet flow rates were conducted (0.125, 0.25, 0.50, and 1.0 g/s). These

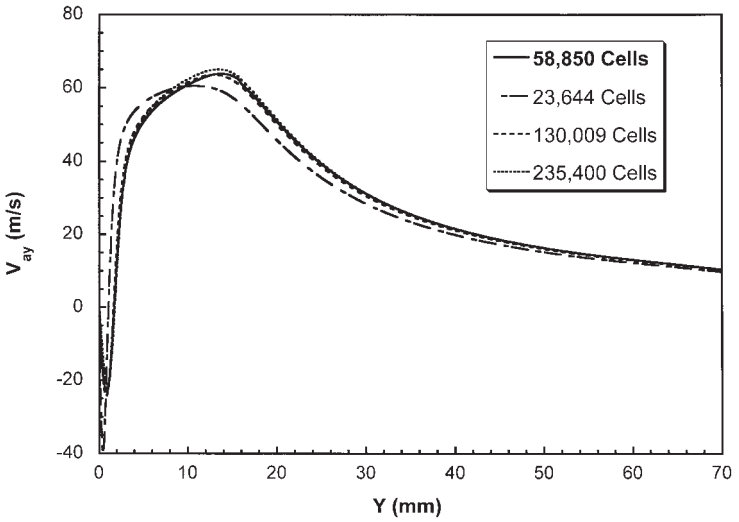

Figure 4 Effect of the grid cell number on the simulated profile of the centerline axial velocity (V_{ay}) for Die A run with an air throughput of 0.25 g/s.

flow rates corresponded to nominal velocities of 30.1 to 289.1 m/s (nominal velocity is defined as the flow rate divided by the cross-sectional area of the annular inlet). The flow rates were chosen such that the flow remained subsonic (the speed of sound in dry air at 21°C and 101 kPa is 343.9 m/s). However, the air flows were high enough so that different levels of compressible behavior could be observed for each die. Table II lists the specific flow rate and die combinations used.

Turbulence modeling and determination of model parameters

The Reynolds stress model (RSM; see Launder et al.[15]) was chosen as the turbulence model for this study. For stationary state and isothermal conditions, the RSM model equation for the transport of Reynolds stresses is given by Durbin and Petterson Reif[16] and FLUENT User's Manual.[6] This equation is:

$$\frac{\partial}{\partial x_k}(\rho U_k \overline{u_i u_j}) = -\frac{\partial}{\partial x_k}[\rho \overline{u_i u_j u_k} + \overline{p(\delta_{kj} u_i + \delta_{ik} u_j)}] + \frac{\partial}{\partial x_k}\left[\mu \frac{\partial}{\partial x_k}(\overline{u_i u_j})\right] - \rho\left(\overline{u_i u_k}\frac{\partial U_j}{\partial x_k} + \overline{u_j u_k}\frac{\partial U_i}{\partial x_k}\right) + \overline{p\left(\frac{\partial u_i}{\partial x_j} + \frac{\partial u_j}{x_i}\right)} - 2\mu \overline{\frac{\partial u_i}{\partial x_k}\frac{\partial u_j}{\partial x_k}} \quad (1)$$

The summation convention is used in the above equation. In addition to the Reynolds stress transport equations, the dissipation rate is modeled by the dissipation equation in the standard k–ε model

$$\rho \frac{D\varepsilon}{Dt} = \frac{\partial}{\partial x_i}\left[\left(\mu + \frac{\mu_t}{\sigma_\varepsilon}\right)\frac{\partial \varepsilon}{\partial x_i}\right] + C_{1\varepsilon}\frac{\varepsilon}{k}G_k - C_{2\varepsilon}\rho\frac{\varepsilon^2}{k} \quad (2)$$

Krutka et al.[3] found in a study of slot melt-blowing dies that the RSM model was more accurate than the k–ε model for modeling the behavior of dual-slot jets. Our simulations of annular dies were tested with the Krutka et al.[3] parameters (which were developed for slot dies). With the Krutka parameters, the simulated annular mean centerline velocity profiles matched the experimental data from annular dies; however, the velocity spreading rates did not match. In fact, the simulated spreading rate was found to be approximately twice that of the experimentally determined spreading rate. Consequently, a study of the effects of different model parameters was undertaken. After testing several different parameter combinations, it was found that changing the value of $C_{2\varepsilon}$ to 1.82 produced the best fit to the experimental velocity correlations proposed by Uyttendaele and Shambaugh.[7]

TABLE II
Die and Flow Rate Combinations Used[a]

	Flow rate (g/s)			
Die	0.125	0.25	0.50	1.0
A	—	X	X	X
B1	—	X	X	X
B3	—	X	X	X
B5	X	X	X	—
C	X	X	—	—
D	X	X	X	—
E	—	X	X	X

[a] X, flow condition simulated; —, flow condition not simulated.

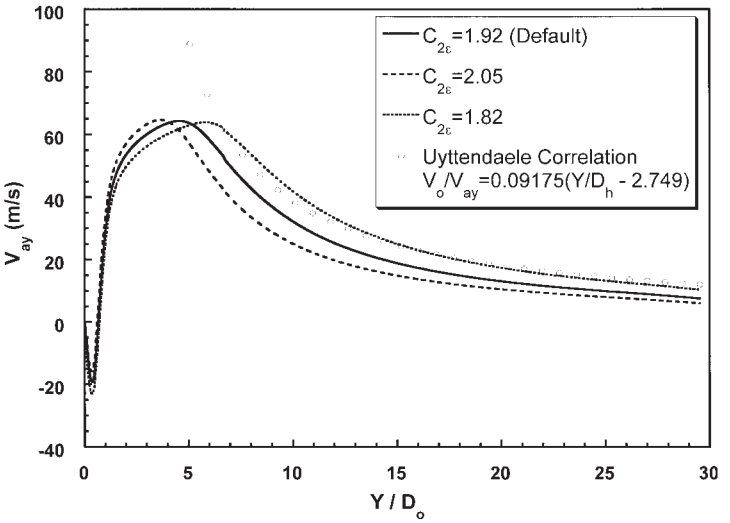

Figure 5 Effect of turbulence parameters on centerline velocity for Die A at an air throughput of 0.25 g/s. In the Uyttendaele correlation, $D_h = D_o - D_i$.

Our $C_{2\varepsilon}$ value of 1.82 is slightly lower than the FLUENT default value of 1.92, whereas the $C_{2\varepsilon}$ value suggested by Krutka et al.[3] is 2.05. In the RSM turbulence model, as well as the standard k–ε model, $C_{2\varepsilon}$ is a constant that controls the magnitude of the rate of dissipation of turbulent energy [see eq. (2)].

In summary, for the RSM model, Fluent recommends the following default values for the nine fitting parameters: $C_\mu = 0.09$, $C_{1ps} = 1.8$, $C_{2ps} = 0.6$, $C'_{1ps} = 0.5$, $C'_{2ps} = 0.3$, $\sigma_k = 1$, $\sigma_\varepsilon = 1.3$, $C_{1\varepsilon} = 1.44$, and $C_{2\varepsilon} = 1.92$. Krutka et al.[3,4] used the first seven of these default parameters. However, they found that changing $C_{1\varepsilon}$ and $C_{2\varepsilon}$ to 1.24 and 2.05, respectively, was necessary to produce a good simulation (based on experimental results) of slot dies used for melt blowing. For our work on the simulation of annular melt-blowing dies, we used eight of the nine parameters used by Krutka et al. However, we had to change $C_{2\varepsilon}$ to 1.82 to produce a good match of the simulation to experimental results. Figure 5 shows a comparison of the centerline velocity calculated using different turbulence model parameters; also shown is the correlation produced by Uyttendaele and Shambaugh[7] from actual experiments with a die of identical geometry. Figure 6 shows the simulated velocity half-widths for the same turbulence model parameters; the correlation suggested by Uyttendaele and Shambaugh is also shown. The velocity half-width ($x_{1/2}$) is the distance from the jet centerline at which the velocity becomes half of its value at the centerline [i.e., $V(x_{1/2}, y) = \frac{1}{2}V_o(0, y)$]. The

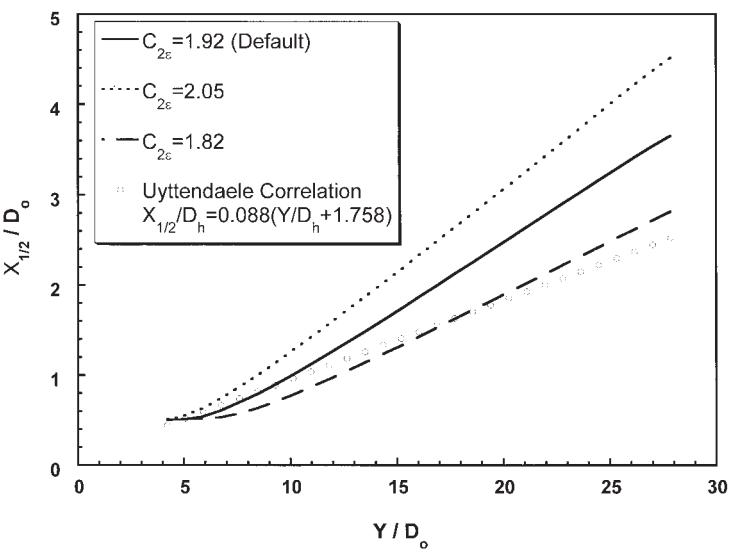

Figure 6 Effect of turbulence parameters on velocity half-width for Die A at an air throughput of 0.25 g/s.

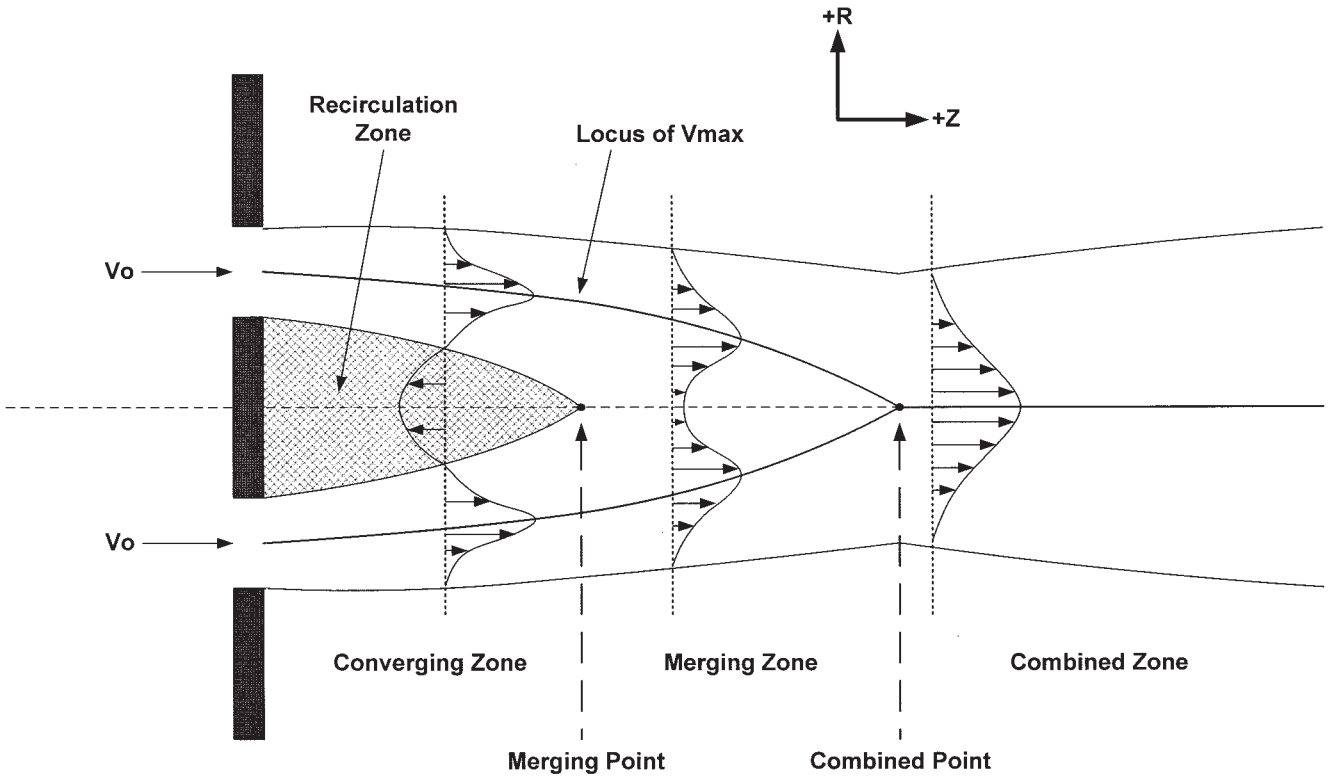

Figure 7 Diagram of near-field flow of an annular jet. This diagram is based on that in Lai and Nasr.[17]

rate of change of $x_{1/2}$ with y is the spreading rate of the jet velocity field. Using $C_{2\varepsilon} = 1.82$ allows us to match correlations (i.e., experimental data) with both the simulated mean centerline velocity and the simulated spreading rate better than using the default model parameters.

Computationally, the CFD analyses discussed here are not expensive. A single run (i.e., the simulation of one die at one flow rate) was completed in about 12 to 18 h using dual 2.2-GHz Xeon processors (Intel, Santa Clara, CA) and approximately 200 megabytes of primary memory.

RESULTS AND DISCUSSION

Centerline velocity correlation

The development of the flow field downstream from an annular jet exhibits three major zones. First, closest to the orifice, is the converging zone, where the jet is still annular in shape. The dominant characteristic of this zone is the presence of a recirculation area where flow is traveling in the opposite direction from the main direction of the jet. The merging zone is next; this is a transition between the converging zone and the fully developed region. The dominant characteristics of the merging zone are the lack of a recirculation area and the presence of peak velocities away from the centerline. The final region is the well-developed region, where the velocity maximum is along the centerline, and the velocity is decaying. Figure 7 shows a diagram of the three zones; Lai and Nasr[17] showed similar zones for parallel jet flow. Figure 8 shows the centerline profile (for Die A run with a high air throughput) with these three zones highlighted. Tanaka[18,19] first reported on and described these three zones for the flow of parallel plane jets. In Figure 8, the point where the centerline velocity crosses from a negative to a positive value is called the merging point; the point where the maximum centerline velocity is reached is called the combined point. These two points were defined by Lai and Nasr.[17]

To better study the centerline velocity profiles, a proper frame of reference is needed to correlate data from various flow rates and flow geometries. In particular, to develop a dimensionless description of the jet behavior, the determination of characteristic scales is needed. The peak centerline velocity (see Fig. 5) was used as the characteristic velocity for the scaling of the centerline velocity. The distance along the centerline from the die face to the point where maximum velocity occurs (i.e., the convergence distance, Z_{max}) was picked to be the characteristic length. The velocity at this point was defined as V_{max}. Note that this is not the maximum velocity in the entire flow field; rather, it is the maximum centerline velocity.

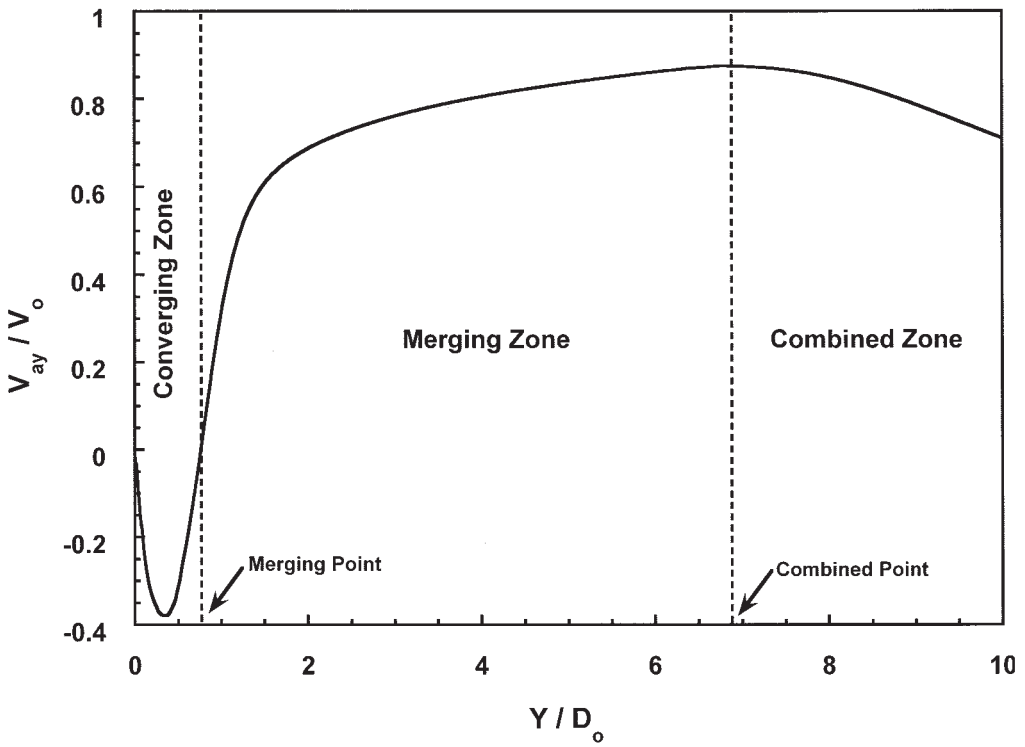

Figure 8 Near-field centerline velocity for Die A at an airflow of 1.0 g/s. The regions of jet development are shown.

To describe the geometry of the jet orifice, three geometric parameters were used. The first parameter is D_o, the outer diameter of the annular opening; the second parameter is D_i, the inner diameter of the annular opening. The third parameter is the fraction open area, *FOA*, which is defined as follows:

$$FOA = \frac{D_o^2 - D_i^2}{D_o^2} \tag{3}$$

The fraction open area is used as a measure of the available flow area versus the flow area of a circular jet with diameter D_o.

To predict the centerline velocity behavior of an annular jet, an empirical model was developed. Through variations of inlet velocity, outer diameter, and fraction open area, a number of different velocity profiles were obtained. These differing velocity profiles served as the basis for developing a universal centerline mean velocity profile. From the computed velocity profiles it was apparent that no simple correlation (e.g., linear, exponential, etc.) could model the behavior of all the variables involved. A slightly more complex correlation was developed using the following equations:

$$V/V_{\max} = F(Z/Z_{\max}) \tag{4}$$

$$Z_{\max}/D_o = G(FOA, V_o/V_{\text{sound}}) \tag{5}$$

$$V_{\max}/V_{\text{sound}} = H(FOA, V_o/V_{\text{sound}}) \tag{6}$$

To determine the mathematical forms for the functions *F*, *G*, and *H*, regression was used based on all the computational cases tested. This analysis showed that the circular die (Die B1) had behavior significantly different from that of the other dies. Therefore, the regression is valid only for the case of annular dies. Regression showed that no simple equation could describe the velocity profile over the entire flow range. The flow field was separated at the point where $V = V_{\max}$ (the "combined point" in Fig. 8), and the two regions were fitted to two different equations. The far-field flow region, where the annular jet is similar to circular jets, was approximated using an inverse linear relationship, given that such a function has been found to describe the decay of centerline mean velocity for circular jets.[11] The second region—the complex near-field flow area—includes both the converging and merging regions. The fitted equations for these regions are

$$\frac{V}{V_{\max}} = c_1 + \frac{c_2}{Z/Z_{\max}} \quad \text{for } Z/Z_{\max} > 1 \tag{7}$$

and

$$\frac{V}{V_{\max}} = ax + bx^2 + cx^3 + dx^4 + ex^5 + fx^6 + gx^7 + hx^8 + ix^9 + jx^{10} \quad \text{for } Z/Z_{\max} < 1 \tag{8}$$

TABLE III
Model Equation Constants That Were Produced by Regression Analysis

Constant	Value	Constant	Value
Equation (7)		Equation (9)	
$c1$	1.2267	α	0.31596
$c2$	−0.05913	β	−0.73194
Equation (8)		Equation (10)	
a	−18.67	A	2.51858
b	373.01	B	6.55777
c	−2661.51	C	1.74253
d	10558.70		
e	−26244.90		
f	42648.80		
g	−45422.30		
h	30612.00		
i	−11855.60		
j	2011.50		

with G defined as

$$\frac{Z_{\max}}{D_o} = \frac{1}{\alpha + \beta FOA^2 + \gamma FOA^3} \tag{9}$$

and H defined as

$$\frac{V_{\max}}{V_{\text{sound}}} = \frac{1}{A + B[FOA^2 \ln(FOA)] + C[\ln(Ma_o)^2]} \tag{10}$$

The values for the regression constants are given in Table III. Figure 9 is an example of how well this empirical model can predict the centerline axial velocity for an annular die for the entire range of y values (die face to far field). Figure 9 shows results for Die B3; results are similar for the other die geometries shown in Table I. As the reader may observe, the match between the correlation and the experiments is excellent. Although theoretical models do exist for the far-field region of flow, very few exist for the important, high-velocity region nearest to the die. Observe that the form for far-field flow is similar to that suggested by Schlichting[11] for the centerline velocity decay of a circular jet.

Velocity spreading and horizontal velocity profile

An important part of modeling the behavior of turbulent jets is capturing the mean velocity spreading rate. The spreading rate is largely dependent on the turbulent transport of momentum away from the jet and the entrainment of additional air mass into the jet from the adjacent quiescent air.

As discussed earlier, the spreading of a turbulent jet is usually characterized by the jet velocity half-width

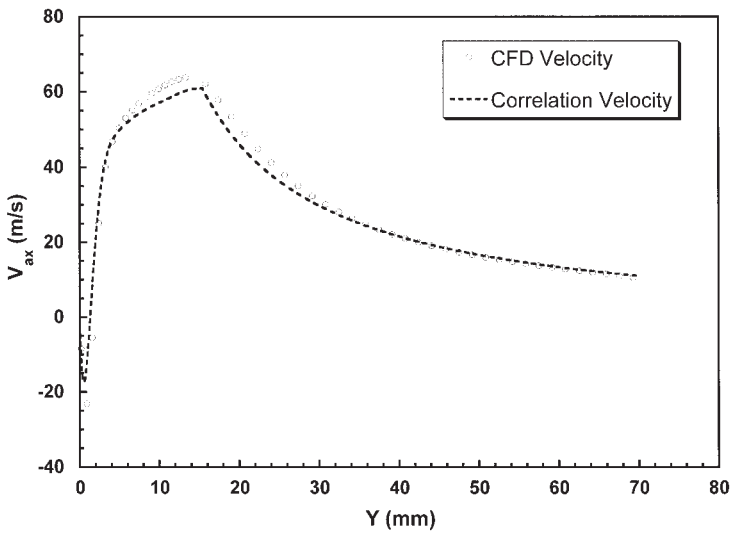

Figure 9 Comparison of centerline axial velocity as predicted by CFD with centerline velocity predicted by empirical correlations [see eqs. (7)–(10)]. These CFD results and correlations are for Die B3 and an airflow of 0.25 g/s.

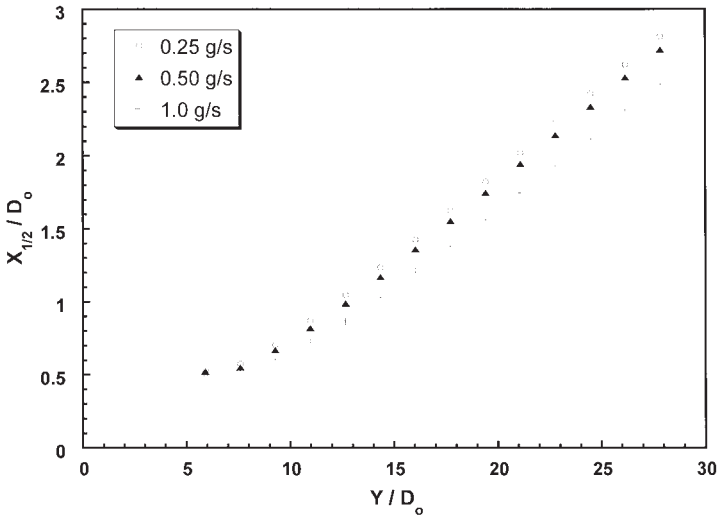

Figure 10 Effect of flow rate on jet spreading for Die A at 0.25, 0.5, and 1.0 g/s.

$x_{1/2}$. The half-width increases with increasing distance from the jet source. Within the well-developed region the growth of the jet is linear.[11] The slope and intercept of this line are measurable characteristics of the jet. For our work both half-width and distance from the die were nondimensionalized using the outer diameter of the die.

The jet spreading rate was calculated for each simulation. To determine the spreading rate constants, the region from $y/D_o = 10$ to the end of the computational domain was used. In every case the velocity half-width varied linearly with position in the well-developed region. Figure 10 shows a typical example (for Die A). It was found that the spreading rate was nearly constant for every case run, including the circular die case (Die B1). Table IV lists the seven dies and the gas flow rates run for each die. The slope and intercept for each of the 19 simulations are listed in the table. The average slope, average intercept, and standard deviations for each die are shown in the last four columns, and the total averages for all the dies are shown at the bottom of the last four columns. A plot of this total average (slope = 0.1139 and intercept = −0.4243) is shown in Figure 11. This average slope is a good representation of our simulations: as Table IV shows, the overall standard deviation of the slope is only 0.0036.

Also shown in Figure 11 are the experimentally determined correlations of four groups of researchers. Our average slope compares well with the experimental work of Majumdar and Shambaugh[13]; they reported a slope of 0.112 and an intercept of 0.040. Uyttendaele and Shambaugh[7] and Obot et al.[8,14] both reported lower values (0.077 to 0.097) for the slope, but they forced the intercept to be zero. With a fixed zero intercept, our data produce an average slope of 0.0935, which is actually within the range given by Obot et al.[14] for circular jets with various inlet geometries. [If we use the FLUENT default turbulent model parameters (curve not shown in Fig. 11), we will produce a line with a slope of 0.146 and an intercept of −0.5528; the fit of this curve to the experimental data is not

TABLE IV
Constants for the Velocity Half-Width Correlations for the Cases That Were Studied

	Flow rate (g/s)											
	0.125		0.25		0.50		1.0		Average		Standard deviation	
Die	Slope	Intercept	Slope	Intercept	Slope	Intercept	Slope	Intercept	Slope	Intercept	Slope	Intercept
A			0.1157	−0.4168	0.1132	−0.4418	0.1052	−0.4629	0.1114	−0.4405	0.0055	0.0231
B1			0.1168	−0.4398	0.1154	−0.4523	0.1108	−0.4456	0.1143	−0.4459	0.0031	0.0063
B3			0.1160	−0.4131	0.1146	−0.4431	0.1080	−0.4375	0.1129	−0.4312	0.0043	0.0160
B5			0.1172	−0.4168	0.1123	−0.4644			0.1148	−0.4406	0.0035	0.0337
C	0.1179	−0.4823	0.1158	−0.5347					0.1169	−0.5085	0.0015	0.0371
D	0.1181	−0.3311	0.1182	−0.3497	0.1147	−0.3653			0.1170	−0.3487	0.0020	0.0171
E			0.1121	−0.3819	0.1113	−0.3861	0.1101	−0.3959	0.1112	−0.3880	0.0010	0.0072
Average	0.1180	−0.4067	0.1160	−0.4218	0.1136	−0.4255	0.1085	−0.4355	0.1139	−0.4243	0.0036	0.0489

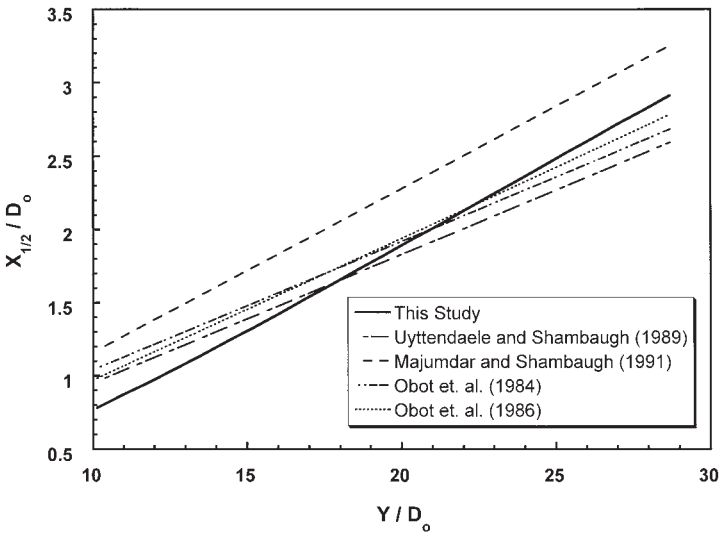

Figure 11 Average half-width (spreading rate) as predicted by CFD. Also shown are experimental jet spreading correlations developed by other researchers.

good.] Discrepancy in the jet spreading correlation is not an unusual occurrence. Kotsovinos[20] reviewed several different works that reported different values for both the slope and intercept of the half-width correlation in plane jets.

As Table IV shows, there is significantly more variance in the intercept than with the slope. Although the overall standard deviation for the slope was only 0.0036, or 3.2%, the intercept had a much larger overall standard deviation of 0.0489, or 11.5%. For a given die geometry our data show that the slope decreases, and the intercept increases, with increasing inlet flow rate. However, when comparing the different die geometries, there is no discernable pattern in the slope or intercept with respect to either inlet velocity or outer die diameter.

Turbulence

The measurement of turbulence quantities is of importance to the melt-blowing process. Strong velocity fluctuations can lead to operating problems, such as the fiber sticking to the die face or the entangling of the newly formed fiber with itself or with adjacent fibers. For very small volumes, such as the near-field region of an annular die, the experimental measurement of turbulence quantities can be difficult. However, regardless of the volume considered, simulations can provide information on the state of turbulence within the flow.

The turbulent kinetic energy (TKE or k) is a measure of the kinetic energy associated with the fluctuations of the velocity; TKE is an output of the FLUENT simulations. Figure 12 shows centerline TKE (nondimensionalized) for Die A at three gas flows. The profiles have a two-peaked shape. The first peak approximately corresponds to the location where the flow reversal ends (see Fig. 7). The second peak corresponds to the region where the centerline velocity is decreasing quickly. For Die A run at 0.25 g/s air flow, Figure 13 shows an overlay of centerline TKE and centerline velocity. The local minimum between the TKE peaks corresponds to the area of highest velocity. Past the second peak, both the TKE and the centerline velocity profile decay. The generation of TKE is proportional to the velocity gradient, so that the areas of highest TKE are also the areas of highest velocity gradient.

It is apparent from Figure 12 that, for Die A, the inlet air flow rate influences both the peak magnitude and the general shape of the curve. The other die geometries show similar results. It appears that this change in the dimensionless TKE is attributed to the growing effects of compressibility on the flow as inlet flow rates increase. With our simulated peak velocities transitioning from the generally accepted incompressible flow regime ($v <$ Mach 0.3) to a compressible regime, this is a reasonable hypothesis to make. (The 0.25, 0.5, and 1.00 g/s flow rates in Fig. 12 correspond to Mach 0.20, 0.40, and 0.80, respectively.) As Figure 12 shows, the peak velocity location and the areas of high velocity gradient move away from the die at higher inlet flow rates. Lau[21] reported that the potential core for compressible circular jets stretches with increasing Mach number. This stretching of the potential core moves the start of velocity decay, and the position of velocity maximum, away from the die face. Thus, it is reasonable to expect that the location of the second TKE peak will move away from the die at higher inlet flow rates.

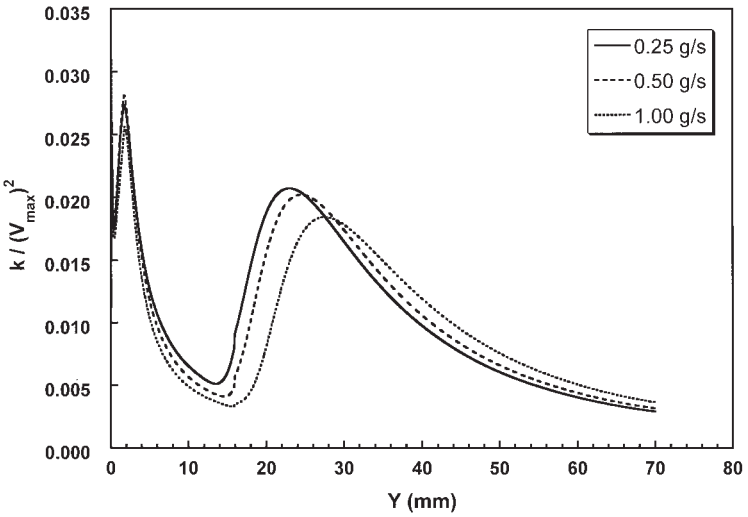

Figure 12 Centerline (dimensionless) TKE versus position for various air flow rates. This simulation is for Die A.

For a given die it is possible to generalize the shape of the TKE curve. For this generalization, TKE is nondimensionalized with SMK, the maximum TKE at the location of the second peak. The abscissa value is nondimensionalized with SMP, the second maximum peak position. With this normalization, the curves for a single die match well. Figure 14 shows this type of plot for Die A. The normalized plots for the other dies look similar to Figure 14. Specifically, the curves for the different airflow rates (for a specific die) are coincident.

The circular die case, Die B1, has a significantly different centerline TKE profile than Die A, which is attributed to the lack of an inner wall and the resulting shear on the flow. Even at very high open areas (e.g., see Die E in Table I), the annular jet turbulence profile is significantly different from that of the circular jet. Figure 15 shows centerline TKE plots for Dies A, B1, and E at an air flow rate of 0.25 g/s. These results suggest that the hypothesis that annular jets can be treated merely as variations on turbulent circular jets is not entirely valid. The presence of the inner wall has a significant effect on the turbulence properties throughout the flow because it is an additional surface of high shear that generates additional turbulence velocity fluctuations. Figure 16 shows the Reynolds stresses along the centerline for Die A at an air flow of 0.25 g/s. It is apparent that the three Reynolds stress curves are different both in shape and magnitude. (There are only three significant Reynolds stresses attributed to the axisymmetric model used for the flow.) The large differences in the Reynolds stresses are an indication that the turbulent flow is anisotropic. The popular k–ε turbulence models, as well as the

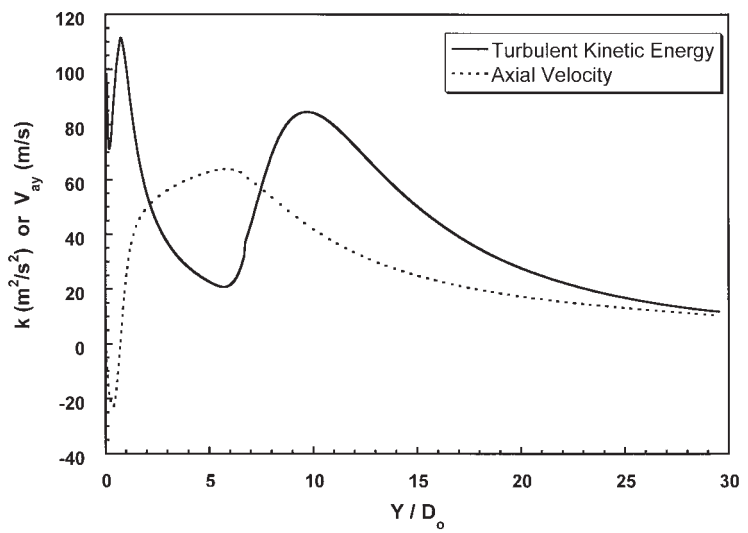

Figure 13 Comparison of centerline TKE and mean velocity for Die A at 0.25 g/s.

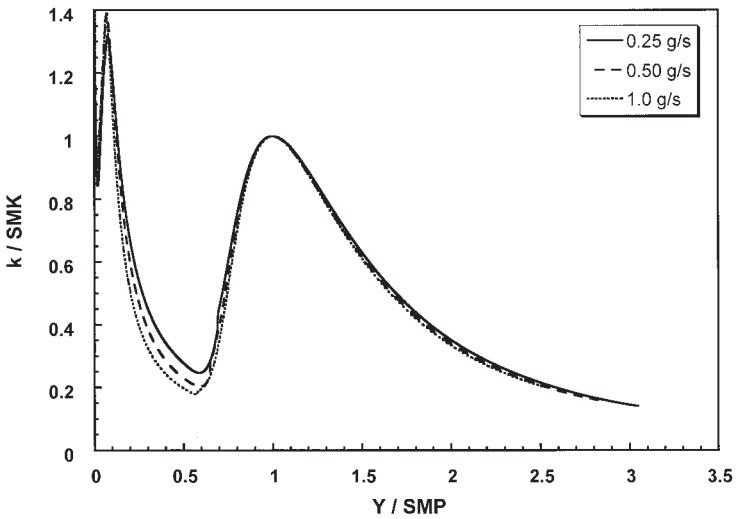

Figure 14 Generalized TKE plot for Die A. SMK = maximum TKE at the location of the second peak. SMP = second maximum peak position.

similar k–ω model, both make the assumption of isotropic turbulence.[16] It has been shown that the k–ε model is not particularly well suited to the flow of turbulent free jets.[3,22] The present work (with the RSM model) suggests that the real flow may have significant turbulent anisotropy, and this anisotropy would hamper the accuracy of the k–ε and k–ω models.

CONCLUSIONS

Through a comparison with experimental data an accurate technique for the simulation of the flow field below an isothermal annular jet has been developed. This technique agrees well with the experimental correlations, it provides insight into annular jet physics, and it is a useful tool for engineering annular jet orifices. At different flow rates a change in flow behavior was observed as the jet velocity progressed through the incompressible to compressible, but subsonic, flow regimes. One observed effect of increasing compressibility seems to be that of extending the area of flow reversal farther from the die face, as well as shifting the velocity peak away from the die.

Rather than using all the FLUENT default parameters, we used a value of 1.24 for $C_{1\varepsilon}$; this value was suggested by Krutka et al.[3] In addition, we set the turbulence parameter $C_{2\varepsilon} = 1.82$, to allow a much better agreement of the simulation with experimental measurements. Specifically, changing the value of $C_{2\varepsilon}$ allowed excellent fits to experimental data of both the centerline velocities and the half-width spreading rate.

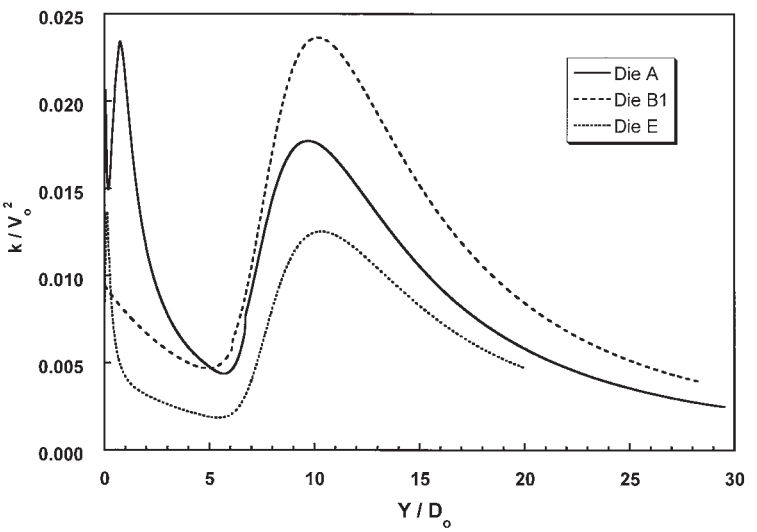

Figure 15 Comparison of (dimensionless) centerline TKE for Dies A, B1, and E at 0.25 g/s.

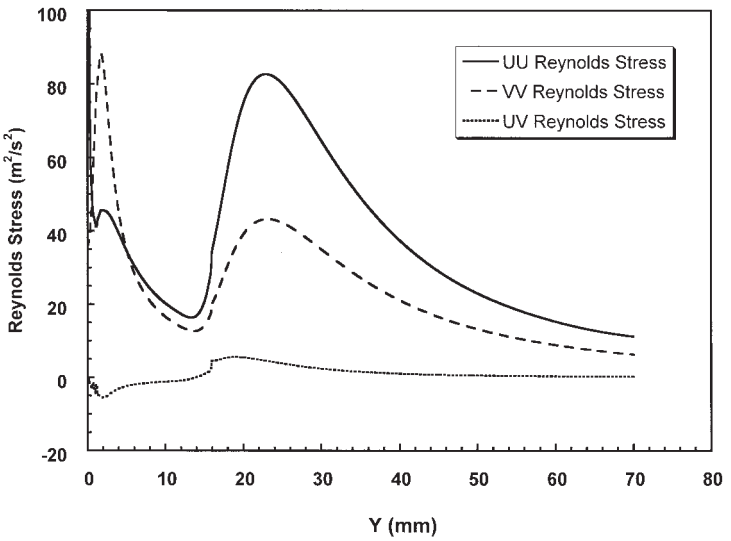

Figure 16 Centerline Reynolds stresses for Die A at 0.25 g/s.

In comparing different air flow rates, it was found that at higher, but industrially operable, air flow rates the effects of compressibility become significant. At large distances from the die, however, it was found that these effects are much smaller than in the near field. When melt-blowing dies are operated at high nominal velocities (velocities $\gtrsim$ 100 m/s), compressibility should be taken into account for the calculation of the air flow field for positions close to the die.

An annular jet has significantly different flow characteristics than those of the more well studied circular jets. The presence of the inner annular wall induces large differences in turbulent behavior. The presence of the recirculation region is the most apparent example of the center wall effects. Another effect of the annular orifice is the large generation of turbulence in the immediate vicinity of the orifice. This turbulence generation is substantially greater for an annular orifice than that for a circular orifice. In addition, the computational results suggest that the turbulence within an annular jet is anisotropic, with larger Reynolds stresses along the axial direction than any cross-direction. This may potentially explain why the common k–ε model does not do a particularly good job of modeling turbulent melt-blowing jets.

NOMENCLATURE

Symbol

Abbreviation **Description**

C_{1ps} coefficient for the slow pressure–strain term of the Reynolds stress model

C_{2ps} coefficient for the rapid pressure–strain term of the Reynolds stress model

C'_{1ps}, C'_{2ps} coefficients for the modeling of the wall reflection effects on the pressure–strain term of the Reynolds stress model

$C_{1\varepsilon}$ parameter for the dissipation equation of the RSM model [eq. (2)[rsqb]

$C_{2\varepsilon}$ parameter for the dissipation equation of the RSM model [eq. (2)[rsqb]

C_μ coefficient for the modeling of turbulent viscosity

D_i inner diameter of annular orifice, mm

D_o outer diameter of annular orifice, mm

D_h difference between inner and outer diameters, $D_o - D_i$, mm

$F(Z/Z_{\max})$ function describing $V_{ay}/V_{\max}$

FOA fraction open area [$FOA = (D_o^2 - D_i^2)/D_o^2$]

$G(FOA)$ function describing $Z_{\max}/D_o$

$H(FOA, Ma_o)$ function describing $V_{\max}/V_{\text{sound}}$

k turbulent kinetic energy [TKE = $\frac{1}{2}(u_i u_i)$], m^2/s^2

Ma_o nominal Mach number ($Ma_o = V_o/V_{\text{sound}}$)

P static pressure, Pa

q turbulence intensity [$q = (u_i^2)^{0.5}/V_o$]

SMK maximum TKE at the location of the second peak (see Fig. 14)

SMP second maximum peak position (see Fig. 14)

TKE ($=k$) turbulent kinetic energy, m^2/s^2

$V_{\max}$ maximum centerline axial velocity, m/s

V_o nominal discharge velocity, m/s
V_{ay} velocity in the y-direction, axial velocity, m/s
V_x velocity in x-direction, m/s
x, y spatial coordinates, mm
$x_{1/2}$ jet half-width defined as the distance from flow centerline at which the mean x velocity becomes half of its value at the centerline, mm

Greek characters

ε dissipation rate of turbulent kinetic energy, m^2/s^3
μ viscosity, kg m^{-1} s^{-1}
ρ local density, kg/m^3
σ_k turbulent Prandtl number for the turbulent kinetic energy
σ_ε turbulent Prandtl number for the rate of dissipation

This work was generously supported by National Science Foundation GOALI Grant DMII-0245324. The authors also are most grateful for the financial assistance provided by 3M, Procter & Gamble, and ConocoPhillips. We also thank Fluent Inc. for providing us with an academic software license.

References

1. Harding, J. W.; Keller, J. P.; Buntin, R. R. U.S. Pat. 3,825,380, 1974.
2. Schwarz, E. C. A. U.S. Pat. 4,380,570, 1983.
3. Krutka, H.; Shambaugh, R. L.; Papavassiliou, D. V. Ind Eng Chem Res 2002, 41, 5125.
4. Krutka, H. M.; Shambaugh, R. L.; Papavassiliou, D. V. Ind Eng Chem Res 2003, 42, 5541.
5. Mukhopadhyay, A.; Prasad, R. O. S.; Grald, J. S.; Lifshutz, N. Performance Analysis of Melt-Blown Dies Using Computational Fluid Dynamics, Proceedings of INTC 2002 Conference, Atlanta, GA, September 25–26, 2002.
6. FLUENT 6.0 User's Guide; www.fluent.com, Fluent Inc.: Lebanon, NH, 2003.
7. Uyttendaele, M. A. J.; Shambaugh, R. L. Ind Eng Chem Res 1989, 28, 1735.
8. Obot, N. T.; Trabold, T. A.; Graska, M. L.; Ganghi, F. Ind Eng Chem Fundam 1986, 25, 425.
9. Rao, R. S.; Shambaugh, R. L. Ind Eng Chem Res 1993, 32, 3100.
10. Marla, V. T.; Shambaugh, R. L. Ind Eng Chem Res 2003, 32, 6993.
11. Schlichting, H. Boundary Layer Theory, 7th ed.; McGraw-Hill: New York, 1979; pp. 729–734, 737.
12. Ferdman, E.; Ötugen, M. V.; Kim, S. J Prop Power 2000, 16, 676.
13. Majumdar, B.; Shambaugh, R. L. Ind Eng Chem Res 1991, 30, 1300.
14. Obot, N. T.; Graska, M. L.; Trabold, T. A. Can J Chem Eng 1984, 62, 587.
15. Launder, B. E.; Reece, G. J.; Rodi, W. J Fluid Mech 1975, 68, 537.
16. Durbin, P. A.; Petterson Reif, B. A. Statistical Theory and Modeling for Turbulent Flows; Wiley: West Sussex, UK, 2001; pp. 147, 149.
17. Lai, J. C. S.; Nasr, A. Proc Inst Mech Eng 1998, 212, 379.
18. Tanaka, E. Bull JSME 1970, 13, 272.
19. Tanaka, E. Bull JSME 1974, 17, 920.
20. Kotsovinos, N. E. J Fluid Mech 1976, 77, 305.
21. Lau, J. C. J Fluid Mech 1981, 105, 193.
22. Pope, S. B. Turbulent Flows; Cambridge University Press: Cambridge, UK, 2000; p. 382.